Self-assembled clusters of patchy rod-like molecules

Miroslav Jurásek,[a,b] **and Robert Vácha**[*a,b]

Supplementary Information

1 Approximation of cluster configuration freedom

Upon aggregation, particles lose part of their freedom of motion, since particles in a cluster have to satisfy the constraints imposed by cluster geometry (see Figure S1). These geometrical constraints can be used to approximate the configurational freedom of clusters.

We start with describing the boundaries on rotation around the main axis, χ_i. From Figure S1, we can immediately see that the angle by which particles can rotate in the cluster can be approximated as

$$\chi_i \approx \alpha_i - \alpha_{min}, \tag{S1}$$

where α_{min} is the minimal angle given by cluster geometry, which is the internal angle of a regular polygon with each vertex corresponding to one particle in the cluster.

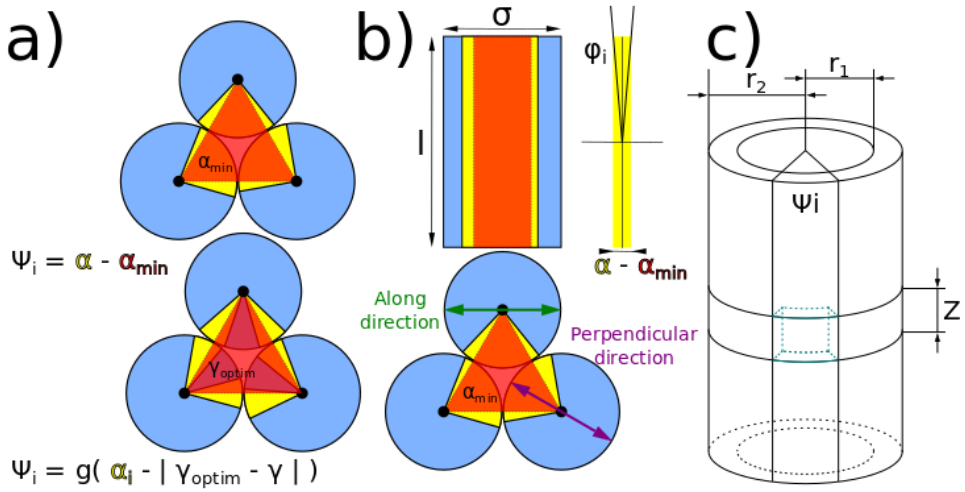

Fig. S1 Schematic illustration of geometrical constraints determining the degrees of freedom of particles in the cluster. Particles are depicted as blue spherocylinders with yellow interaction patches. a) top view of regular closed trimer of one patch particles (top) and two-patch particles (bottom). The red triangle shows the necessary patch size to form regular closed trimers, while the remaining yellow parts depict the angle within which each particle could rotate in the cluster. b) side projection of the patchyspherocylinder from the cluster center (top-left) and top view of the trimer (bottom) with two directions of particle rotations. (top-right) depicts the angle, ϕ_i, by which the particle can lean out along the patch. c) binding volume defined as volume accessible to the center of mass of an interacting particle. z describes the freedom of movement along the axis of the first particle. r_1 is the radius of the inner cylinder, roughly equal to the radius of the particle ($\sigma/2$), r_2 is the radius of the outer cylinder, that is defined by the interaction range. ψ_i is the effective interaction patch size ($\alpha_i - \alpha_{min}$).

Rotational freedom perpendicular to the patch (see Figure S1) is mostly dependent on the interaction potential (e.g. its range and shape). The orientational freedom along the patch is mainly a function of patch size α and could be approximated as

$$\phi_i \approx 2\arctan\left[\frac{\sigma}{l}\sin\left(\frac{\delta}{2}\right)\right], \tag{S2}$$

where $\delta = \alpha_i - \alpha_{min}$, σ is the particle diameter, and l is its length. In the first approximation we can use a Taylor expansion of Eq (S2) around $\delta = 0$:

$$\phi_i \approx 0 + \frac{\sigma}{l}\delta + O(\delta^2). \tag{S3}$$

The translation of a particle in the cluster is restricted to the binding volume (see Figure S1) , which is the wedge-shaped segment of space centred and aligned on the first particle that determines the motion of the second particle. The binding volume is:

$$V_i \approx \pi z(r_2^2 - r_1^2)(\alpha_i - \alpha_{min}), \tag{S4}$$

where z is the height of the cylinders, given by the range in which the second particle can fluctuate along the axis of the first particle, r_1 and r_2 being the radius of the inner and outer cylinder given by the minimal and maximal distance between the centers of both interacting particles, respectively (see c) in Figure S1).

In total the degrees of freedom of the particles in the cluster can be approximated as:

$$V_i\chi_i\phi_i \approx A_i g(\alpha_i - \alpha_{\min})^{3w_i}, \tag{S5}$$

where A_i is the factor including all other contributions independent of the patch size, w is the scaling factor and $g(x) = x$ for $x > 0$ and 0 otherwise.

2 Theoretical structure diagram

Theoretical equipopulation lines in structure diagrams could be derived from a combination of Eq (1), Eq (3), and the law of mass action for the arbitrary pair of cluster k and j as

$$\begin{aligned} K_{j,k} = \frac{e^{-\beta(\langle E_j\rangle - \langle E_k\rangle)}}{(8\pi^2)^{j-k}} \left(\frac{\sigma_k}{\sigma_j}\sigma_1^{j-k}\right) \\ \left(\frac{v_j}{v_k}v_1^{k-j}\right) \frac{\prod_{i=1}^{j} V_i\chi_i\phi_i}{\prod_{i=1}^{k} V_i\chi_i\phi_i}, \end{aligned} \tag{S6}$$

where $K_{j,k} = \frac{n_j}{n_k}n_1^{k-j}$. Or it can be rewritten to express temperature:

$$T = \frac{\langle E_j\rangle - \langle E_k\rangle}{k_B \ln\left(\frac{n_k}{n_j}n_1^{j-k}(8\pi^2)^{k-j}\left(\frac{\sigma_k}{\sigma_j}\sigma_1^{j-k}\right)\left(\frac{v_j}{v_k}v_1^{k-j}\right)\frac{\prod_{i=1}^{j} V_i\chi_i\phi_i}{\prod_{i=1}^{k} V_i\chi_i\phi_i}\right)}. \tag{S7}$$

Eq (S6) could be reformulated to separate the values obtainable from simulations: average populations, n_i, and energies, E_i (on the left side) and fitted parameters (on the right side): excluded volume, multiplicative constant A_i, and scaling factor w_i:

$$\begin{aligned} \ln\left(\frac{n_j}{n_k}n_1^{k-j}\right) + \beta(\langle E_j\rangle - \langle E_k\rangle) = \\ (k-j)\ln\left(8\pi^2\right) + \ln\left(\frac{\sigma_k}{\sigma_j}\sigma_1^{j-k}\right) + \\ \ln\left(\frac{v_j}{v_k}v_1^{k-j}\right) + \ln\left(\frac{\prod_{r=1}^{j} V_i\chi_i\phi_i}{\prod_{r=1}^{k} V_i\chi_i\phi_i}\right). \end{aligned} \tag{S8}$$

Importantly, we validated the individual components in Eq (S8) by simulations, where only certain parameters were modified, e.g. concentration or patch size.

2.1 Effect of concentration

The concentration effect could be derived from Eq (S8) for low concentrations, where we approximate the system as a gas of clusters with only excluded volume interactions and assume that the internal configuration entropy of cluster is independent of concentration. If we assume that the volume accessible to any cluster is the same $v_j = v_k = v_1 = V - V_{exclude}$, we can evaluate

the change in the translation entropy between clusters of different size as

$$\begin{aligned}\Delta S(V,\alpha) &= k_B \ln\left(\frac{v_j}{v_k} v_1^{k-j}\right) + k_B \ln\left(\frac{\prod_{r=1}^{j} V_i \chi_i \phi_i}{\prod_{r=1}^{k} V_i \chi_i \phi_i}\right) \\ &\quad - k_B \ln\left((8\pi^2)^{j-k} \frac{\sigma_j}{\sigma_k} \sigma_1^{k-j} \frac{n_j}{n_k} n_1^{k-j}\right) \\ &= k_B (k-j) \ln(V - V_{exclude}) + \Delta S(\alpha) + const.\end{aligned} \tag{S9}$$

where k_B is the Boltzmann constant, j and k are sizes of clusters, V is the volume of the system, and $V_{exclude}$ is the volume not accessible to clusters or monomers.

Eq (S9) could be rewritten to express change in the translation entropy of particles upon aggregation into cluster of size j where we chosen $k = 1$

$$\Delta S(V) = k_B (1-j) \ln(V - V_{exclude}) + const. \tag{S10}$$

Magnitude of exclude volume per particle is generally dependent on size of the cluster j, morphology of the cluster, density of the system, and its cluster composition. However as an bottom boundary for exclude volume per particle we can take volume per spherocylinder in regular close packing given by $V_{cp} = \sigma^3 \left(\frac{1}{\sqrt{2}} + \frac{\sqrt{3}}{2} \frac{l}{\sigma}\right)$. Our effective exclude volume should be higher then close packing and should converge to close packing limit at high densities.

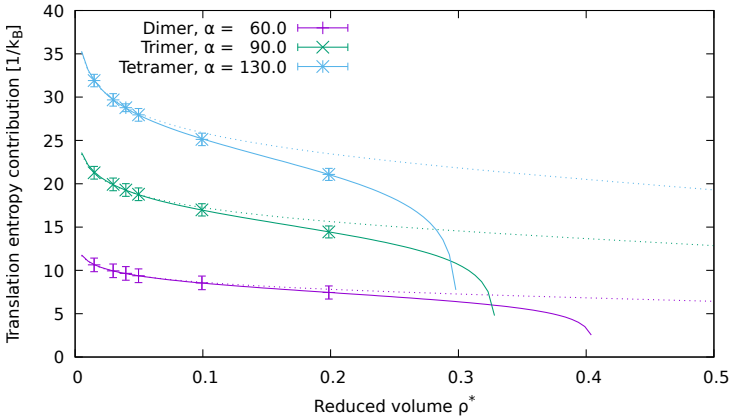

Fig. S2 Translation entropy lost of monomers upon aggregation into clusters as function of reduced density $\rho^* = NV_{cp}/V$. Points are simulated data with error bars equal to standard deviations. Filled lines correspond theoretical fits to the simulation data. Dotted lines corresponds to excluded volume of spherocylinders in regular close packing, V_{cp}.

We can see that the simulated change in translational entropy for dimers, trimers, and tetramers can be fitted well by Eq (S9) using an effective excluded volume ($\rho_{ex} \approx 0.407\ \rho^*$ for dimers, $\rho_{ex} \approx 0.330\ \rho^*$ for trimers, and $\rho_{ex} \approx 0.300\ \rho^*$ for tetramers). At very low concentrations (below 0.1 ρ^*), the excluded volume has no effect and systems can be well described as ideal gas. At concentrations around 0.2 ρ^* the excluded volume starts to play a role, but stays below the close packing limit as anticipated.

2.2 Effect of patch size

The change in the configuration entropy of a particle upon aggregation into various clusters can be expressed from Eq (S7) as the following function of patch size:

$$\begin{aligned}\Delta S(\alpha) &= k_B \ln\left(\prod_{r=1}^{j} V_i \chi_i \phi_i\right) \\ &= k_B \sum_{i=1}^{j} \ln(A_i g(\alpha_i - \alpha_{min})^{3w_i}),\end{aligned} \tag{S11}$$

where we used Eq (5). The expression can be further simplified for regular symmetric clusters, where all particles are equivalent:

$$\Delta S(\alpha) = k_B j \ln(Ag(\alpha - \alpha_{min})^{3w}), \tag{S12}$$

which could be used to fit scaling constant w and multiplicative constant A. The theory fits the simulated data very well in Figure S3. From the fit we obtained the scaling factors, w and multiplicative constant A (see Tab. 1). For dimers and trimers we achieved $w_2 = 0.4395$ and $w_3 = 0.4282$, respectively. In limiting case, where all particles are parallel the scaling factor should be $w \leq 2/3$, because particles lost at least one degree of freedom involving α.

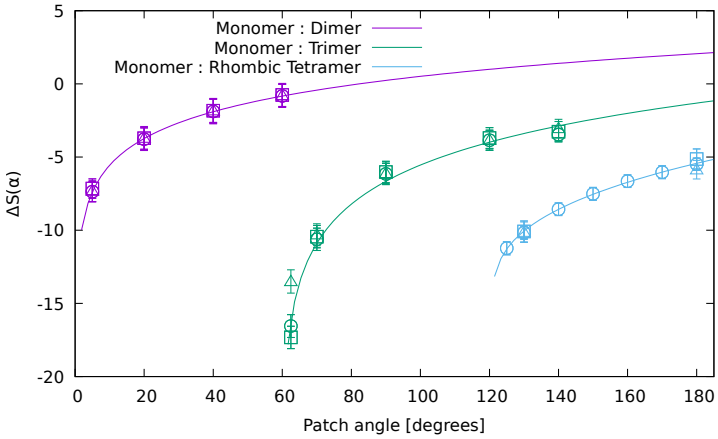

Fig. S3 Comparison between theoretical (lines) and simulated (points) changes in configuration entropy as a function of patch size ($\Delta S(\alpha)$). Data are shown for three reduced densities: squares for $\rho \approx 0.015\ \rho^*$, circles for $\rho \approx 0.040\ \rho^*$, and triangles for $\rho \approx 0.199\ \rho^*$. We can see that theory fits simulation data well and data for all densities overlap. Therefore, we can conclude that the change of configuration entropy as function of patch size is independent on density for densities smaller then $0.199\ \rho^*$.

In symmetric clusters all particles are equal, however this is not true in asymmetric rhombic tetramers where particles in the middle (closer to center of mass of the cluster) and on sides differ in number of contacts and degree of rotational freedom around particle axis (see particles in the middle and on sides of rhomboid in 3). This way entropy change in the rhomboid tetramer is given as

$$\begin{aligned} \Delta S \quad &= 2k_B \ln(A_m g(\alpha_i - \alpha_m)^{3w_m}) \\ &+ 2k_B \ln(A_s g(\alpha_i - \alpha_s)^{3w_s}) \end{aligned} \tag{S13}$$

where s denotes particles at sides, m denotes particles in the middle, and angles $\alpha_m = 60.0^\circ$ or $\alpha_s = 120.0^\circ$ are minimal angles for particle on side and in the middle, respectively. Theory fits the simulated data well (blue line and points in Figure S3). From fit we obtained scaling factors $w_m = 0.6883$, $w_s = 0.2231$ and multiplicative constant $A_s = A_m = A = 4.6650\ 10^{-4}$.

The fitted parameters obtained can be used to reconstruct structure diagram as the function of patch size and concentration/density. We demonstrated this in Figure 4 and in Figure S4, where theoretical and simulation data are in good agreement. The only deviation from theory was observed for larger patch sizes and at higher densities. The deviations are most probably caused by small change in the mean cluster energy which is assumed to be constant in the theory. Because the equilibrium constant is exponentially dependent on the mean cluster energy, even small changes of the energy could have an impact on approximated cluster population in the theory (see Figure S5). Therefore, one should be careful about using the theory to extrapolate the conditions where cluster mean energy changes significantly. Another contribution for theory and simulation differences from could arise from lager chain-like clusters which are not included in the theory.

3 Fitting of structure diagrams

The theory was used to fit equipopulation points from the simulations of particles with different patch sizes. For one patch particles with short-range interactions, the parameters were fitted also to the points obtained at various densities. Equipopulation

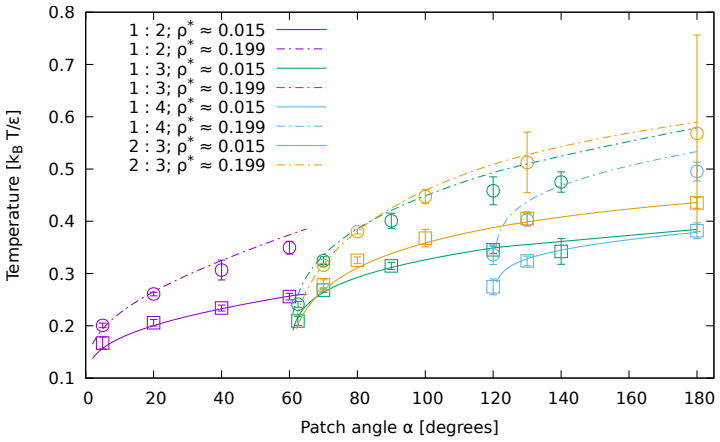

Fig. S4 Comparison between the simulated and calculated structure diagram of particles with one patch and short range interactions at two different densities. Lines are calculated from the theory with parameters obtained by fitting (see Table 1). Circles and squares correspond to the equipopulation points from simulations at densities $\rho \approx 0.015\rho^*$ and $\rho \approx 0.199\rho^*$, respectively. Equilibirum populations between monomers and dimers, trimers, and tetramers are displayed by violet, green, and light blue colors, respectively. Orange corresponds to the same populations of dimers and trimers. Theory and simulation data deviate little at larger densities and large patch sizes.

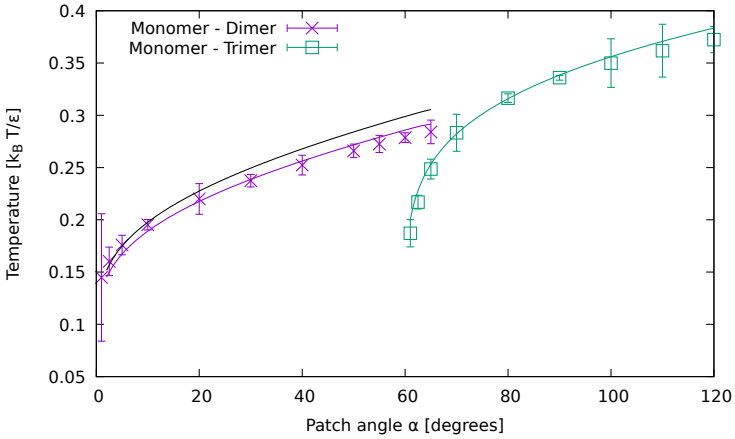

Fig. S5 Comparison of calculated and simulated structure diagram for dimers and trimers. Lines are calculated from the theory while points represent simulation results at density $\rho \approx 0.04\ \rho^*$. Colored lines correspond to the mean energy of dimers and trimers $\langle E_2 \rangle = -2.64\ k_BT$ and $\langle E_3 \rangle = -7.9\ k_BT$, respectively. Black line corresponds to the extrapolation using mean interaction energy from low patch sizes $\langle E_2 \rangle = -2.85\ k_BT$. The best agreement between the theory and simulations is obtained for mean energy averaged over all patch angles.

line between monomers and clusters of size j could be derived from Eq (S7) as:

$$T = \frac{\langle E_j \rangle}{k_B \sum_{i=1}^{j} \ln(A_i g(\alpha_i - \alpha_{min})^{3w_i})} \tag{S14}$$

Fitted parameters from the structure diagram of particles with one or two patches and short or farther reaching interaction are in Tables I to IV.

4 Illustrative examples of clusters

We defined clusters as a group of particles interacting together stronger than a threshold (1.4 ε) and all the particles can be interconnected together via these interactions. As a result removing any particle from cluster decreases the total interaction

	Dimer	Trimer	Rhombic Tetramer
E $[k_BT]$	-2.64	-7.85	-13.15
w	0.4395	0.4282	0.6883
w_2	-	-	0.2231
A	2.9818 10^{-3}	1.3768 10^{-3}	4.6650 10^{-4}
ρ^*_{ex}	0.4072	0.3300	0.2998

Table 1 Fitted parameters for systems with particles with one patch and short range interactions used in Figure 4 A.

	E $[k_BT]$	w	A
Dimer	-2.62	0.3914	2.1640 10^{-4}
Trimer	-7.73	0.5319	1.1476 10^{-5}
Cross Tetramer	-16.35	0.4977	1.3567 10^{-6}
Pentamer	-26.33	0.6588	1.3747 10^{-8}

Table 2 Fitted parameters for systems with particles with one patch and farther reaching interactions used in Figure 4 B.

	E $[k_BT]$	w	A
Trimer	-8.62	0.4202	2.5666 10^{-6}
Tetramer	-11.47	0.3708	3.0642 10^{-7}
Pentamer	-14.25	0.6547	6.9880 10^{-9}
Hexamer	-17.10	0.2304	1.3817 10^{-8}

Table 3 Fitted parameters for systems with particles with two patched and short range interactions used in Figure 5.

	E $[k_BT]$	w	A
$\alpha = 10.0°$, $d = 0.3$ nm	-8.40	0.4095	3.5649 10^{-6}
$\alpha = 20.0°$, $d = 0.3$ nm	-8.40	0.3739	1.0554 10^{-5}
$\alpha = 10.0°$, $d = 1.0$ nm	-8.40	0.5510	1.0423 10^{-6}

Table 4 Fitted parameters of trimers for systems with particles with two patched and short range interactions used in Figure S9.

energy of the cluster and the cluster cannot be split to two without the decrease of the interaction energy (see Figure S6). Threshold value was used to remove random clusters from consideration. In our case we chose value 1.4ε, so that dimers with such interaction energy would be at least four times more populated then pair of monomers at temperature $1kT/\varepsilon$. Note that ε is the interaction strength of patch per unit length. In our description of particles with two patches we concluded that for each angle between patches γ, the most stable cluster geometry is such geometry where particles have maximal freedom of rotation around its axis. For example for $\gamma = 90.0°$ we assumed optimal geometry being tetramer with cross section of regular square. Except small regular clusters, e.g. square cluster, more complex geometries can satisfy the geometrical condition for closed clusters (see b in Figure S6). Therefore, we investigated cluster morphology during the determination of cluster stability. Larger clusters are entropically disfavoured and are expected to appear at high concentrations.

5 Parallel approximation in regular clusters

We defined a regular cluster as a cluster where spherocylinders were parallel with an angular deviation of less than 20°. We tested the validity of this definition by investigation of a mean angle of spherocylinders in the dimer. Dimer was selected as the most fluctuating cluster. We varied the spherocylinder length from 2 to 16 and the patch size from 5°up to 60°, while we kept the energy of optimal cluster the same. In Figure S8 we can see average angle rapidly decreases with the increasing length. The

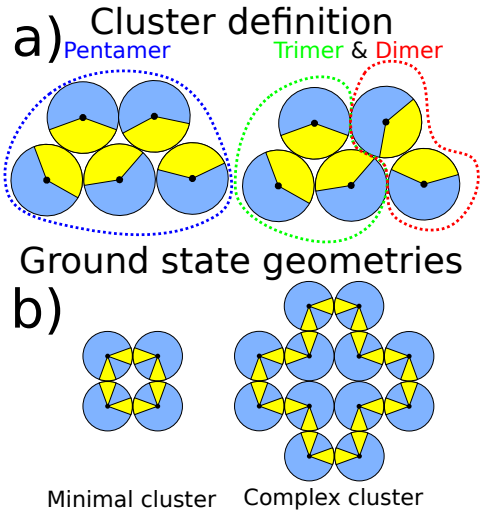

Fig. S6 Illustration of cluster definitions. a) Two particles belong to the same cluster if they attract each other, i.e. it is largest aggregate with no way to split without losing interaction energy. There is an example of a pentamer on the left and two clusters (a dimer and trimer) on the right. b) There are two examples of closed regular clusters for an angle between patches $\gamma = 90°$. The left example is the tetramer, the minimum size of the cluster. The right example is a dodecamer. Since large clusters are very rare, most stable regular closed clusters are also clusters minimal in size.

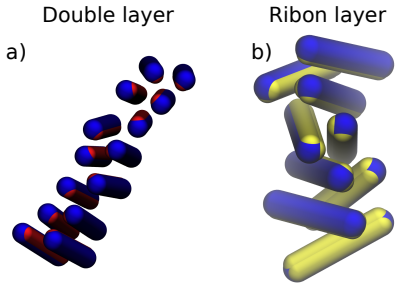

Fig. S7 Depiction of two types of fibrillar structures formed by patchy spherocylinders with one interaction patch at low temperatures for patch sizes a) 140°and b) 280°.

regular clusters with our definition are almost all clusters for length larger and equal 3.

6 Effect of interaction range and patch size

We investigated the effect of the interaction range and patch size on the structure diagram of clusters formed by two patch spherocylinders (see Figure S9). Larger interaction range resulted in stabilization of clusters with the very similar behavior. The increase of patch size resulted in the broader region of γ and slight stabilization of the clusters, where closed trimers could be obtained. Such effects were anticipated based on the cluster geometry.

7 Distribution of clusters close to structural boundaries

Interesting rich behaviour was observed for one patch particles close to the structural boundaries of 60 and 120°. The change of the system composition with temperature is depicted in Figure S10. Similar effect has the interaction strength, which suggests that for these particles the dominant cluster size can be easily tuned.

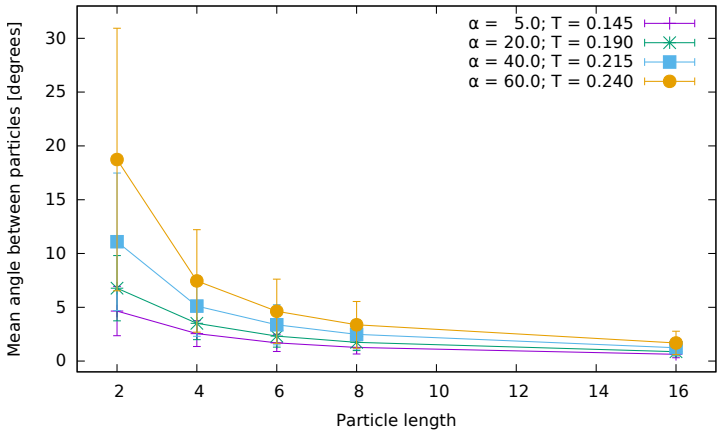

Fig. S8 Mean angle between the particles in dimer as a function of spherocylinders aspect ratio. Various patch sizes are depicted. Systems were simulated at the equipopulation temperature with respect to monomers.

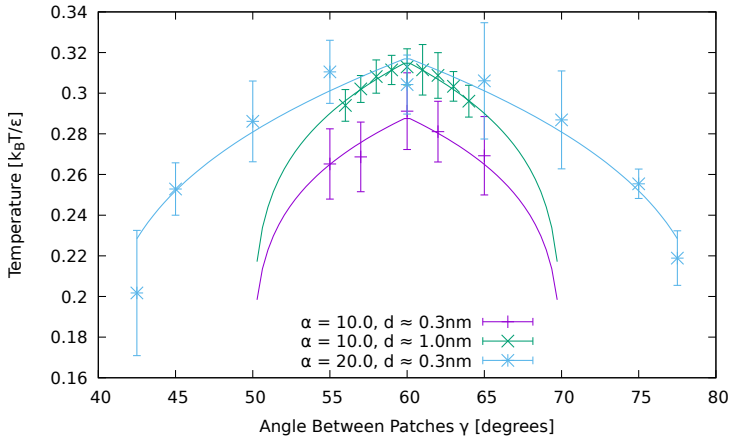

Fig. S9 Equipopulation lines between monomers and closed trimers formed by two patch spherocylinders. Magenta line corresponds to spherocylinders with short-range interaction (≈ 1.64nm) and small patch size ($\alpha_1 = \alpha_2 = 10.0^\circ$). Blue stands for the spherocylinders with larger patch size ($\alpha_1 = \alpha_2 = 20.0^\circ$) and green is for the spherocylinders with the increased range of interaction ($d \approx 2.30$nm). Error bars represent one standard deviation in cluster population fluctuation during the simulation.

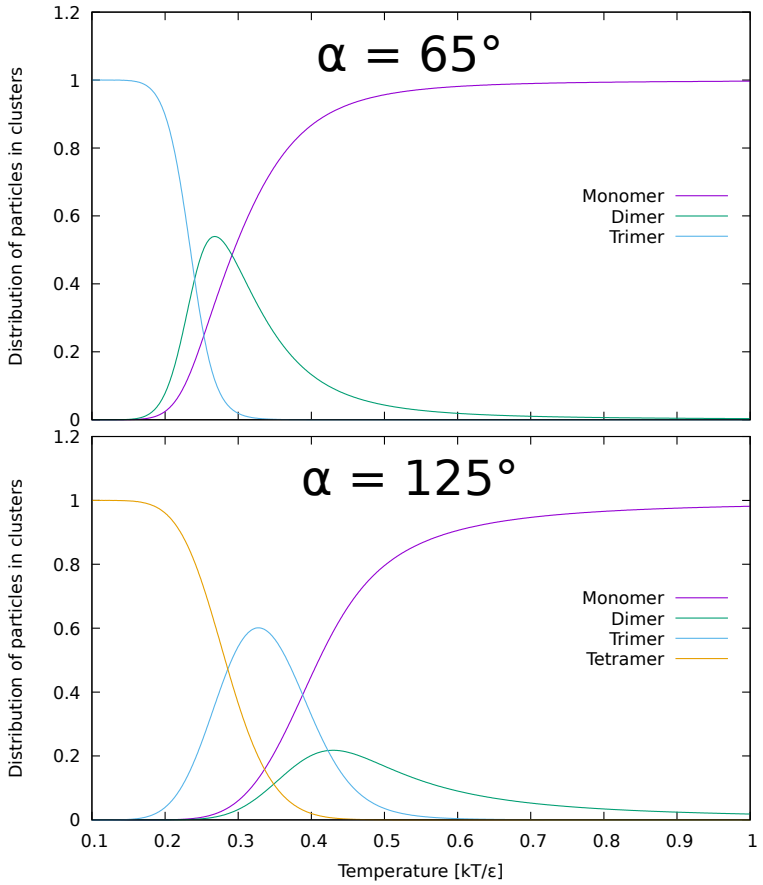

Fig. S10 Distribution of particles in clusters of different size as function of reduced temperature. Curves are calculated from theory for two patch sizes in region where transition between clusters of different sizes are observed. In top graph we have patch size of 65°and at bottom for 125°. Graphs corresponds to reduced density $\rho^* \approx 0.040$.